

HNPS Advances in Nuclear Physics

Vol 28 (2021)

HNPS2021



${}^6\text{Li}(n,t)\alpha$ reaction event-identification for the ${}^{235}\text{U}(n,f)/{}^6\text{Li}(n,t)$ cross section ratio measurement in the NIFFTE fissionTPC

Maria Anastasiou

doi: [10.12681/hnps.3567](https://doi.org/10.12681/hnps.3567)

Copyright © 2022, Maria Anastasiou



This work is licensed under a [Creative Commons Attribution-NonCommercial-NoDerivatives 4.0](https://creativecommons.org/licenses/by-nc-nd/4.0/).

To cite this article:

Anastasiou, M. (2022). ${}^6\text{Li}(n,t)\alpha$ reaction event-identification for the ${}^{235}\text{U}(n,f)/{}^6\text{Li}(n,t)$ cross section ratio measurement in the NIFFTE fissionTPC. *HNPS Advances in Nuclear Physics*, 28, 30–35. <https://doi.org/10.12681/hnps.3567>



${}^6\text{Li}(n,t)\alpha$ reaction event-identification for the ${}^{235}\text{U}(n,f)/{}^6\text{Li}(n,t)$ cross section ratio measurement in the NIFFTE fissionTPC

M. Anastasiou^{1,*}

For the NIFFTE Collaboration

¹ Lawrence Livermore National Laboratory

Abstract While nuclear data play an important role in nuclear physics applications, it has become important to have a better understanding of the data and try to minimize the uncertainties. In particular, there is a need for precision neutron-induced fission cross section measurements on fissile nuclei. Neutron-induced fission cross sections are typically measured as ratios, with a well-known standard in the denominator. While the ${}^{235}\text{U}(n,f)$ reaction is a well measured standard, some light particle reactions are also well-known and their use as reference can provide information to remove shared systematic uncertainties that are present in an actinide-only ratio. A recent measurement of the ${}^{235}\text{U}(n,f)$ reaction using as a reference the standard ${}^6\text{Li}(n,t)$ reaction, was conducted at the Los Alamos Neutron Science Center using the NIFFTE collaboration's fission time projection chamber (fissionTPC). The fissionTPC is a $2\times 2\pi$ charged particle tracker designed for measuring neutron-induced fission. Detailed 3D track reconstruction of the reaction products enables evaluation of systematic effects and corresponding uncertainties which are less directly accessible by other measurement techniques. This work focuses on the analysis for the event identification of the ${}^6\text{Li}(n,t)\alpha$ reaction in the fissionTPC.

Keywords ${}^{235}\text{U}$, ${}^6\text{Li}$, Time Projection Chamber

INTRODUCTION

Nuclear data plays an important role in both defense and energy related applications. These systems have become increasingly dependent on advanced simulation and modeling. The accuracy of these models are no better than the underlying uncertainties of the nuclear data they use. It is therefore imperative that nuclear data uncertainties are minimized and well-understood. Specifically, there is a need for precision neutron-induced fission cross-section measurements on fissile nuclei such as ${}^{239}\text{Pu}$. The NIFFTE collaboration, comprised of two national laboratories and four universities, has developed the fissionTPC to measure energy-differential neutron-induced fission cross-section ratios with the goal of total uncertainties less than 1% (both statistical and systematic). For comparison, traditional measurements using ionization chambers are limited to 3–5% total uncertainty. The primary goal of the fissionTPC project is to measure the ${}^{239}\text{Pu}(n,f)$ cross section to sub-1% accuracy. Providing precision measurements requires extensive effort and a methodical approach. To this end the fissionTPC project has made a series of detector development and validation measurements [1], [2].

Ultimately the uncertainty of any cross-section ratio measurement is limited by the uncertainty of the reference standard. The ${}^1\text{H}(n,n)$ elastic scattering cross section is the most accurate neutron standard. However, the ${}^6\text{Li}(n,t)\alpha$ reaction, another neutron cross section standard, has many advantages compared to ${}^1\text{H}(n,n)$ from a detection standpoint: solid, thin targets in the form of LiF can be made with relative ease; the large Q-value of 4.8 MeV provides sufficient energy for a fast cathode timing signal for nToF; and the two charged particles emitted in the reaction provide an excellent event tag and background suppression in a TPC. Taken together these advantages make sub-percent measurement uncertainties with the fissionTPC much more achievable than for a ${}^1\text{H}(n,n)$ measurement. We measure the ${}^{235}\text{U}(n,f)/{}^6\text{Li}(n,t)\alpha$ cross-section ratio as a precursor development measurement to a

* Corresponding author, email: anastasiou2@llnl.gov

$^{239}\text{Pu}(n,f)/^{6}\text{Li}(n,t)\alpha$ cross-section ratio.

EXPERIMENTAL SET-UP

The fissionTPC works on the basic principle that electrons will drift through a gas at a fixed average velocity when in a uniform electric field. By segmenting the anode and instrumenting each segment with a separate channel, a 2-D image of the charge cloud generated by an ionizing particle projected on the anode can be reconstructed (see Fig. 1 – right). By monitoring the relative arrival time of each signal the 3rd dimension of the track can then be reconstructed. The particle tracking information can help determine sample uniformity, beam profile, and other parameters which were often estimated rather than measured in previous measurements. In addition, it also enables improved discrimination of fission fragments, alphas and other charged particles. An extensive description of the fissionTPC can be found in Ref. [3].

The fissionTPC consists of two gas-filled detection volumes viewing a single central target (see Fig. 1 – left). The two cylindrical volumes are filled with a mixture of argon with 5% CO_2 at a pressure of 600 torr. The target is mounted on the central plane, which acts as a cathode. The target for measuring the $^{235}\text{U}(n,f)/^{6}\text{Li}(n,t)$ consists of an approximately $0.4\ \mu\text{m}$ thick ^{6}LiF deposit and a $0.1\ \mu\text{m}$ thick $^{235}\text{UF}_4$ deposit on a $1\ \mu\text{m}$ thick aluminum backing. The Al foils were mounted on $0.5\ \text{mm}$ thick target rings by the Lebow Company. The ^{6}LiF was vapor deposited at LLNL and the $^{235}\text{UF}_4$ was vapor deposited at Oregon State University. The ^{235}U target thickness was selected based on experience gained with previous targets used at LANSCE and the ^{6}Li thickness was set to match the expected counting rate of $^{235}\text{U}(n,f)$ events at 5 MeV. The Al backing is transparent to α -particles and tritons from $^{6}\text{Li}(n,t)$ reaction.

The experiment was conducted at the Los Alamos Neutron Science Center (LANSCE) Weapons Neutron Research (WNR) facility on the 90L flight path [4]. The LANSCE facility provides a pulsed white neutron source. For this experiment the pulses were delivered at 100 Hz. Each pulse of approximately $625\ \mu\text{s}$ length consisted of micro-pulses spaced by $1.8\ \mu\text{s}$. A neutron time-of-flight measurement was employed to determine incident-neutron energies.

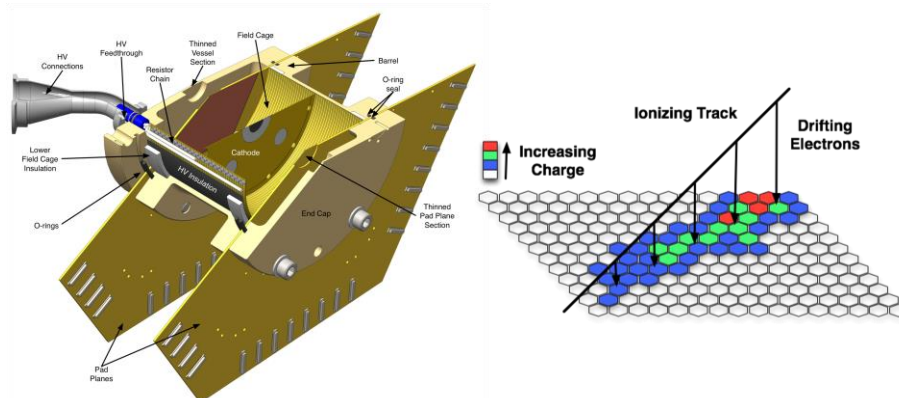


Fig. 1. (Left) A cut-away of the fissionTPC detector. Details can be found in Ref. [3]. (Right) A schematic representation of the fissionTPC data reconstruction. Each hexagonal segment of the anode is instrumented and the signal size and time are recorded.

$^{6}\text{Li}(n,t)\alpha$ EVENT IDENTIFICATION

A myriad of neutron beam-induced charged-particle reactions are detected in the fissionTPC. The majority of these particles are in the proton band, which includes deuterons and tritons, followed by α -particles (see Fig. 2). The reactions are a result of beam interactions with the detector housing and drift gas, and constitute a background for detecting the $^{6}\text{Li}(n,t)\alpha$ reaction products. The vast majority of

these background reactions however, are not two-particle coincident reactions occurring at the central cathode plane. Furthermore, the relative angle between the particles from a ${}^6\text{Li}(n,t)\alpha$ reaction are dictated by reaction kinematics. This means that the chance of an accidental coincidence between two background reactions, such as (n,p) and (n,α) in the detector gas, that have a shared vertex and also fall within the allowed kinematic phase space is small. Fig. 2 – right shows a visual reconstruction of a ${}^6\text{Li}(n,t)\alpha$ reaction in the fissionTPC, while Fig. 2 – left shows the track length vs. energy spectrum of the data.

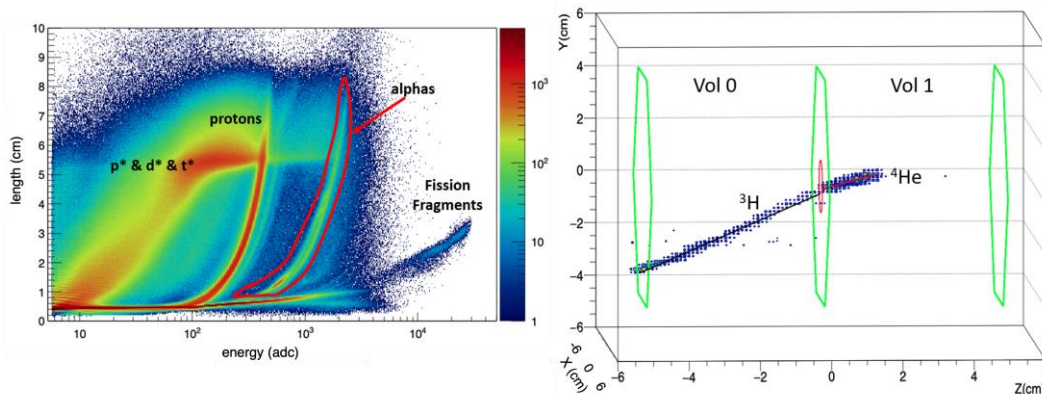


Fig. 2. (Left) Track length vs. energy for the ${}^{235}\text{U}(n,f){}^6\text{Li}(n,t)$ data. The α -band selection gate is shown. The particle band labeled p^* etc. is composed of the proton, deuteron, and triton tracks that have enough energy to extend the full active area of the detector volume, therefore depositing only a portion of their energy. (Right) Visualization of the reaction products from the ${}^6\text{Li}(n,t)\alpha$ reaction in the fissionTPC. The α -track is fully contained within the TPC active volume, while the triton traverses the entire depth of the detector. The start vertices and start time of both tracks are coincident.

By selecting two-track events with shared vertices and gating on the α -band, the ${}^6\text{Li}(n,t)\alpha$ events can be identified. Fig. 3 shows the α -band selection and the corresponding triton tracks identified as having a shared vertex and being within the expected angular range. A variety of background reactions can be seen, likely from beam-induced accidental coincidences or alternative $n+{}^6\text{Li}$ reaction channels, particularly at lower triton energies.

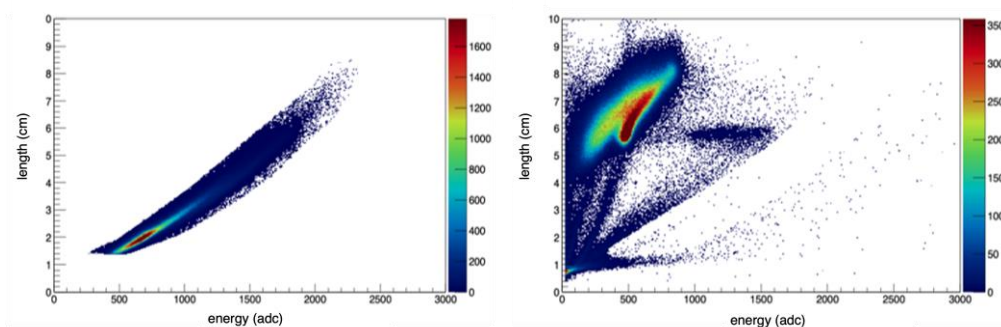


Fig. 3. The α -band selection cut (left) and the corresponding triton tracks (right) that also pass the shared vertex and angular selections. Background reactions from alternative ${}^6\text{Li}+n$ reaction channels and beam-induced accidental coincidences can also be seen, particularly at lower energies.

As a reaction with a two-body final state, the angular relationship and energy sharing between the triton and α -particle are given by simple kinematic considerations. As an example, Fig. 4 – left shows the kinematic relationship between the polar angle of the α -particle on the y-axis and triton pair on the x-axis, for neutron energies between 0.1 – 4.0 MeV. The exact relation of the polar angles will change

as a function of incident neutron energy. For the same energy limits, as the kinematics calculation confirms on Fig. 4 – right, the final state particles are mainly emitted back-to-back. To take advantage of the two-particle background suppression, both particles must be identified. Even with a thin backing there will be some angular ranges for which the α -particles and/or tritons lose most or all of their energy. A selection on particle angles in ranges where energy loss is minimized is therefore applied, causing the empty regions in Fig. 4 – left.

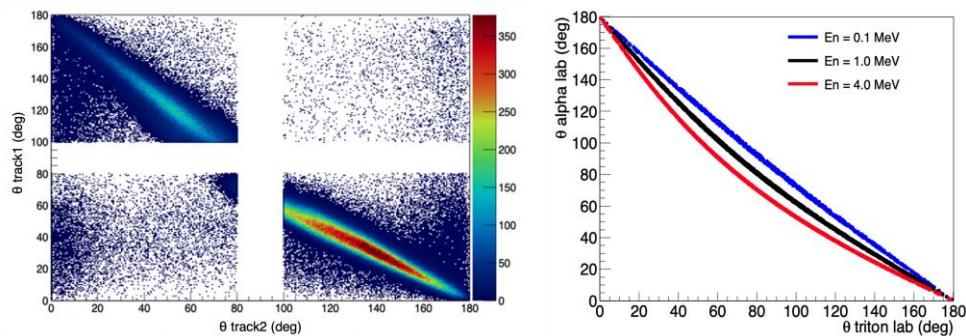


Fig. 4. (Left) The angular correlation for the ${}^6\text{Li}(n,t)\alpha$ events in the data for a range of neutron energies. The empty regions in the center of the angular range is due to an additional angular selection cut. (Right) The angular correlation between the particles in the ${}^6\text{Li}(n,t)\alpha$ determined by a kinematics calculation for single incident neutron energies.

An additional event identifier that can be used to distinguish the ${}^6\text{Li}(n,t)\alpha$ reaction events from background reaction channels is the Q-value. Events from the ${}^6\text{Li}(n,nd)\alpha$ channel that is open beyond 1.8 MeV neutron energies will be present in the data. Using the deposited energies and polar angles of the selected alpha particles from the selection cuts, and the neutron energy of the recorded event, the Q-value of the ${}^6\text{Li}(n,t)\alpha$ reaction is reconstructed as it is demonstrated in Fig. 5 - left. The main peak is the Q-value of the ${}^6\text{Li}(n,t)\alpha$ events. The shift from the nominal value of 4.8 MeV is due to the alpha particle energies not being corrected for energy loss as they go through the solid target. The structure around -2 MeV occurs due to misreconstructed ${}^6\text{Li}(n,nd)\alpha$ events. These data structures were verified with a Geant4 Monte Carlo simulation that takes into account reaction kinematics for two- and three-body reaction channels, reaction cross sections, and detector effects such as energy loss, scattering, anode gain, and dead channels. Fig. 5 - right shows a simulation of the ${}^6\text{Li}(n,t)$ and ${}^6\text{Li}(n,nd)$ reactions, pointing to the small amount of deuterons on the length vs energy space that remain after the shared vertex and angular selection cuts are imposed.

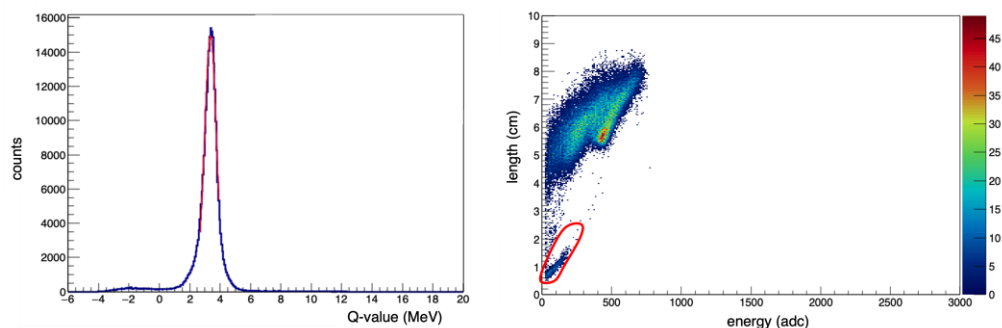


Fig. 5. (Left) Reconstructed Q-value for the ${}^6\text{Li}(n,t)\alpha$ reaction. The main peak corresponds to the ${}^6\text{Li}(n,t)$ reaction Q-value, while the events around -2 MeV are due to misreconstructed alphas from the ${}^6\text{Li}(n,nd)$ channel. (Right) Geant4 Monte Carlo simulation of the ${}^6\text{Li}(n,t)$ and ${}^6\text{Li}(n,nd)$ channels. The red-circled region are deuterons from the ${}^6\text{Li}(n,nd)$ channel remaining after the applied selection cuts.

DISCUSSION

The performance of the ${}^6\text{Li}(n,t)\alpha$ event identification cuts is verified through the Geant4 MC simulation. Fig. 6 shows the ratio of ${}^{235}\text{U}(n,f)$ experimental data to simulated ${}^6\text{Li}(n,t)$ events compared to the ENDF/B-VIII.0 cross section ratio. The comparison between the ${}^{235}\text{U}(n,f)$ -data/ ${}^6\text{Li}(n,t)$ -simulation ratio and ENDF establishes that the ${}^{235}\text{U}(n,f)$ events are being accurately counted and that the 240 keV resonance is well reconstructed. In order to establish the event identification performance the simulated ${}^6\text{Li}(n,t)$ and ${}^6\text{Li}(n,nd)$ events are processed through the selection cuts previously described. Up to 1 MeV neutron energies the shape ${}^{235}\text{U}(n,f)$ -data/ ${}^6\text{Li}(n,t)$ -simulation ratio follows the ENDF/B-VIII.0 cross section ratio. Small discrepancies can occur due to the fact that different sources of events (experimental data and simulation) are being compared; that is why error bars of statistical uncertainty would be meaningless to be assigned at this stage. Differences at higher reaction energies between curves (1) and (2) are due to selection efficiency corrections that are not taken into account for the demonstration of this comparison. For the small amount of the ${}^6\text{Li}(n,nd)$ events that remain after our selection cuts (see Fig. 5), the simulation showed that they correspond to larger than 3 MeV neutron energies so they are not contributing to the curves (1) and (2) of Fig. 6.

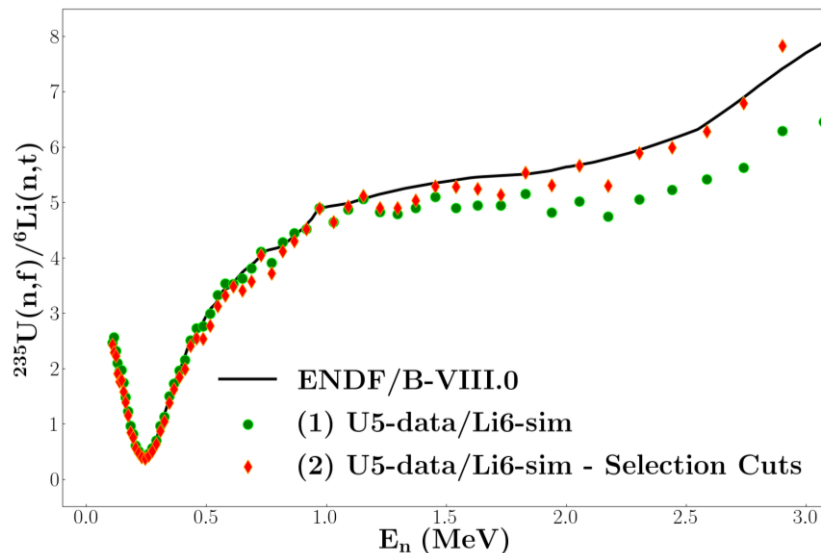


Fig. 6. Performance of the ${}^6\text{Li}(n,t)\alpha$ -reaction event selection using simulated ${}^6\text{Li}(n,t)$, as well as ${}^6\text{Li}(n,nd)$ events. The ratio of ${}^{235}\text{U}(n,f)$ experimental data to simulated ${}^6\text{Li}+n$ events is compared to the ENDF/B-VIII.0 cross section ratio before (1) and after (2) the simulated ${}^6\text{Li}+n$ events are processed through the shared-vertex, α -band and angular selection cuts. The plot establishes that the ${}^{235}\text{U}(n,f)$ events are being accurately counted, the 240 keV resonance is well reconstructed and the ${}^6\text{Li}(n,t)\alpha$ reactions are properly identified among background reactions.

In conclusion, the performance plot verifies that by utilizing the detailed particle coincident tracking in the fissionTPC and the reaction kinematics' unique signatures the ${}^6\text{Li}(n,t)\alpha$ reaction events are successfully identified. For the final experimental ${}^{235}\text{U}(n,f)/{}^6\text{Li}(n,t)$ cross-section ratio a detailed efficiency calculation will be implemented in the fissionTPC Geant4 framework simulation. A model, that includes reaction kinematics for two- and three-body reaction channels, cross sections and angular distributions, and detector effects such as energy loss, scattering, anode gain, and dead channels, will be tuned to minimize the χ^2 -fit to the various particle trends in the data (angle-angle, energy-angle, energy-length) in order to extract the selection efficiency due to the shared-vertex cut, the α -band cut and the angular selection cut

Acknowledgments

This work was performed under the auspices of the U.S. Department of Energy by Lawrence Livermore National Laboratory under Contract DE-AC52-07NA27344. (LLNL-PROC-828168)

References

- [1] R. J. Casperson et al., *Phys. Rev. C* 97, p. 166 (2018)
- [2] L. Snyder et al., arXiv:2107.02881v1, (2021)
- [3] M. Heffner et al., *NIMA* 759, p. 50 (2014)
- [4] P. W. Lisowski et al., *NIMA* 562, p. 910 (2006)